doi:10.1006/jmbi.2000.3727 available online at http://www.idealibrary.com on IDEAL® J. Mol. Biol. (2000) 299, 421–429

JMB

Cross-linking Constraints on F-actin Structure

Eldar Kim[1], Willy Wriggers[2], Martin Phillips[1], Kevin Kokabi[1] Peter A. Rubenstein[3] and Emil Reisler[1]*

[1]*Department of Chemistry and Biochemistry and the Molecular Biology Institute, University of California, Los Angeles CA 90095, USA*

[2]*Department of Molecular Biology, The Scripps Research Institute, La Jolla CA 92037, USA*

[3]*Department of Biochemistry University of Iowa College of Medicine, Iowa City IA 52242, USA*

**Corresponding author*

The DNase I binding loop (residues 38-52), the hydrophobic plug (residues 262-274), and the C terminus region are among the structural elements of monomeric (G-) actin proposed to form the intermonomer interface in F-actin. To test the proximity and interactions of these elements and to provide constraints on models of F-actin structure, cysteine residues were introduced into yeast actin either at residue 41 or 265. These mutations allowed for specific cross-linking of F-actin between C41 and C265, C265 and C374, and C41 and C265 using dibromobimane and disulfide bond formation. The cross-linked products were visualized on SDS-PAGE and by electron microscopy. Model calculations carried out for the cross-linked F-actins revealed that considerable flexibility or displacement of actin residues is required in the disulfide cross-linked segments to fit these filaments into model F-actin structures. The calculated, cross-linked structures showed a better fit to the Holmes rather than the refined Lorenz model of F-actin. It is predicted on the basis of such calculations that image reconstruction of electron micrographs of disulfide cross-linked C41-C374 F-actin should provide a conclusive test of these two similar models of F-actin structure.

Keywords: F-actin; structure; cross-linking; disulfide bonds; protein dynamics

Introduction

The original version of the widely accepted Holmes *et al*. (1990) model of F-actin structure was derived by fitting the atomic structure of G-actin (complexed to DNase I) to X-ray fiber diffraction data of oriented actin gels of about 8 Å resolution. Two subsequent refinements of this model (Lorenz *et al*., 1993; Tirion *et al*., 1995) preserved its main features, albeit some changes were introduced in the location of several structural elements on actin. The most significant changes that resulted from the refinements by using a directed mutations algorithm (Lorenz *et al*., 1993), or the normal modes of the monomer structure (Tirion *et al*., 1995), were in locations and orientations of the DNase I binding loop (D-loop; residues 38-52 in subdomain 2) and the C-terminal segment of actin. Compared to the Holmes model of F-actin structure (Holmes *et al*., 1990), the Lorenz model (Lorenz *et al*., 1993) proposed lower axial and radial locations for the D-loop. All three models of F-actin structure account for many experimental observations and are consistent with low-resolution image reconstructions of electron micrographs of F-actin and acto-S1 complexes (Rayment *et al*., 1993; Schröder *et al*., 1993; Milligan *et al*., 1990). However, they have yet to be tested in experiments aimed at providing experimental constraints on interdomain and intermolecular interactions in F-actin. Such constraints are needed for further refinements of F-actin structure and for addressing the reservations about the Heidelberg models (Holmes *et al*., 1990; Lorenz *et al*., 1993; Tirion *et al*., 1995) that were raised by Chik *et al*. (1996). These constraints will also be useful for assessing the role of F-actin dynamics, and especially at its intermolecular interfaces in actin function.

Three flexible structural elements of actin molecule were selected for the first round of disulfide formation-based testing of F-actin structure. The D-loop, the C terminus, and the hydrophobic plug on actin (H-plug; residues 262-274) were targeted for these experiments either because of their proposed interactions with each other (Holmes *et al*., 1990; Lorenz *et al*., 1993; Tirion *et al*., 1995; Owen & DeRosier, 1993), or the differences between their

Abbreviations used: DBB, dibromobimane; EM, electron microscopy.

E-mail address of the corresponding author: reisler@mbi.ucla.edu

0022-2836/00/020421–9 $35.00/0

location in the Holmes (Holmes *et al*., 1990) and Lorenz (Lorenz *et al*., 1993) models. The D-loop in actin's subdomain 2 assumes special importance in the considerations of F-actin structure. Biochemical observations, including those on His40 and Gln41 labeling (Hegyi *et al*., 1974; Kim *et al*., 1996), D-loop cleavage (Schwyter *et al*., 1990; Khaitlina *et al*., 1993) and BeF_x^- effects on F-actin (Muhlrad *et al*., 1994), and the structural work of Orlova & Egelman (1993) reveal an important role for this loop in F-actin structure and function, and suggest that the D-loop may equilibrate among different conformational states. The possible role of such dynamic changes in subdomain 2 in the regulation of actin by tropomyosin and troponin has been discussed in a review by Squire & Morris (1998). In a recent study on intermolecular cross-linking of Gln41 to Cys374 in F-actin (*via* azidonitrophenyl putrescine), the D-loop was immobilized and linked with a 11.1-12.5 Å spacer to the C terminus of an adjacent actin monomer (Hegyi *et al*., 1998). Such a cross-linking inhibited the ability of actin to generate force and motion with myosin (Kim *et al*., 1998a). This finding implicated dynamic transitions in subdomain 2 on actin in the actomyosin motor functions. The intermolecular coupling of the D-loop and the C terminus (Orlova & Egelman, 1995; Kim & Reisler, 1996) and of the H-plug and the C terminus (Feng *et al*., 1997) has also been suggested.

To map intermolecular interfaces in F-actin and provide experimental constraints on models of F-actin structure, targeted cysteine cross-linking in actin filaments was pursued in this study by using yeast actin mutants with the Q41C and S265C substitutions. Double-site mutants Q41C/C374S and S265C/C374A, in which the reactive Cys374 was also replaced, were used for the preparation of F-actin co-polymers in which the proximity of the D-loop and H-plug could be tested. The similar structures of yeast and skeletal actins, as judged by their monomeric structures and by the EM images of F-actin (Belmont *et al*., 1999) justify the use of yeast actin here.

Results and Discussion

Intermolecular cross-linking in F-actin

The goal of this work has been to assess the possibility for direct interactions between the D-loop, the C terminus, and the H-plug within the same intermolecular interface in F-actin (Tirion *et al*., 1995; Owen & DeRosier, 1993), by measuring the distances between these structural elements in cross-linking experiments. To this end, we prepared (see Materials and Methods) new yeast actin mutants Q41C (with Gln41 replaced by a cysteine residue) and Q41C/C374S (with both Gln41 and Cys374 mutations), and also employed the previously described S265C and S265C/C374A yeast actins (Feng *et al*., 1997). The disulfide and/or dibromobimane cross-linking experiments were carried out on these actin mutants and on the wild-type yeast actin. The cysteine residue pairs 41-374 and 265-374 (and 41-265) were targeted for cross-linking despite a significant separation of these residues in the models of F-actin structure (~11 Å for the 41-374 pair in the Holmes model, and ~20 Å for all other pairs in the Holmes and Lorenz models). Our selection was based on the structural flexibility of these sites and the prior spectroscopic (Feng *et al*., 1997) and chemical cross-linking evidence for their spatial proximity (Kim *et al*., 1998a).

To verify that disulfide bonds are specifically formed only between the reactive cysteine residues 41, 265, and 374 on F-actin, two control tests were performed. In the first test, wild-type actin and the mutants carrying a single reactive cysteine residue (Q41C/C374S and S265C/C374A) were exposed to identical oxidation conditions and the same subsequent treatment and analysis as the Q41C and S265C F-actin. Figure 1 shows that such actins do not form disulfide and dibromobimane cross-linked oligomers, as monitored by SDS-PAGE under non-reducing conditions, except for trace amounts of dimers. In the second test, monomers (G-actins) of all actins used in this study were oxidized and analyzed as described above. The G-actins did not form disulfide and dibromobimane-linked oligomers (data not shown) except for trace amounts of dimers that might be produced by small amounts of aggregated or denatured actin.

Figure 2 shows the results of disulfide and dibromobimane (DBB) cross-linking of the mutant F-actins. For the cysteine residue pairs C41-C374 and C265-C374 (panels 1 and 2), the two cross-linking reactions (disulfide and DBB) reached the same plateau, corresponding to approximately 95 and 60 % of cross-linked actin, respectively, and showed identical distribution of oligomers on SDS-PAGE. A comparison of DBB cross-linked oligomer bands visualized by Coomassie blue staining (Figure 2) and UV fluorescence (not shown) revealed a similar distribution of the intensities of both signals among different bands, irrespective of the reaction time. This suggests that there is little, if any, accumulation of actin species with a monofunctionally attached DBB, and that the cross-linking step of the reaction is fast relative to the initial modification of actin by DBB. The different timescales of the disulfide ($CuSO_4$ catalyzed) and DBB cross-linking of F-actin (Figure 2) reflect different experimental protocols used in the two reactions (to avoid cysteine oxidation in the DBB reaction) and the rate-limiting initial attachment of DBB to actin. Similar extents of spontaneous disulfide cross-linking of these actins are reached after 60 minutes or 15 hours, depending on experimental conditions (see Materials and Methods). These considerations suggest that the 41-374 and 265-374 cysteine residue pairs on adjacent monomers in F-actin can be linked equally well with a short and rigid DBB spacer (7.2 Å) or a disulfide bond,

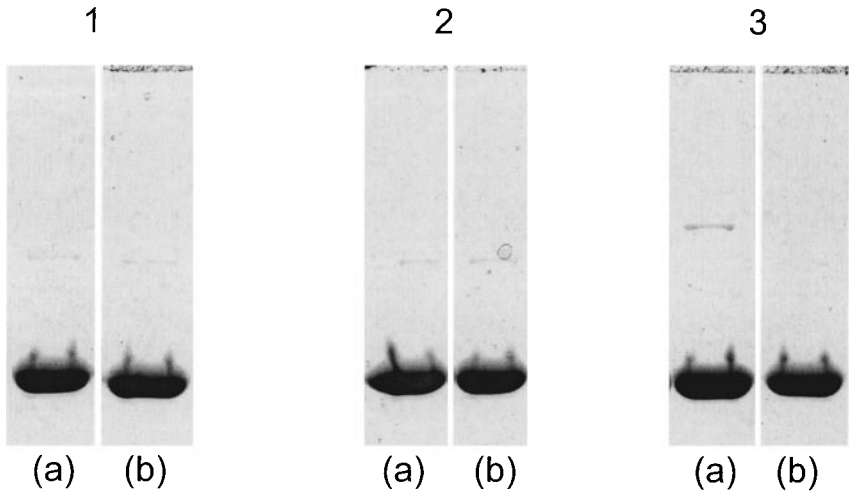

Figure 1. SDS-PAGE (non-reducing) of yeast F-actins after oxidation or reaction with dibromobimane. Panels 1-3 correspond to wild-type (C374), Q41C/C374S (C41), and S265C/C374A (C265) F-actins, respectively. All actins contain a single reactive cysteine residue per monomer (indicated in parentheses). Disulfide bond formation (lanes a) was catalyzed over two minutes by 50 μM $CuSO_4$. Dibromobimane cross-linking (lanes b) was carried out for 90 minutes. Only trace amounts of cross-linked dimers, corresponding to small amounts of aggregated or denatured actin can be detected on these gels.

which is indicative of the mobility of the cross-linked sites. Structural flexibility at this intermolecular interface in F-actin is also highlighted by the transglutaminase mediated cross-linking of Q41 to C374 in skeletal α-actin with a 11-12.5 Å long reagent, *N*-(4-azido-2-nitrophenyl) putrescine (Hegyi *et al*., 1998).

The electrophoretic mobilities of the S265C and Q41C cross-linked oligomers are markedly different. This is not surprising, since the shape of the cross-linked oligomers and their electrophoretic mobilities depend on the sites of cross-linking (the S265C oligomers show similar migration on SDS PAGE to those of *p*-phenylenedimaleimide cross-linked oligomers; data not shown). The observation that the Q41C and S265C actins are cross-linked to different extents and the fact that the reactions do not proceed to completion implies that partial cross-linking of filaments restricts their flexibility and local motions that favor such a reaction. The implicit connection between the different extent of Q41C and S265C F-actin cross-linkings and the hypothesized inhibition of their internal dynamics is consistent with the modeling of the cross-linked F-actins (see below).

Figure 2 (panel 3) also shows the results of cross-linking the co-polymers of the Q41C/C374S and S265C/C374A actin mutants. In this case, the cross-linking connects the D-loop and H-plug on monomers located on the opposite strands of

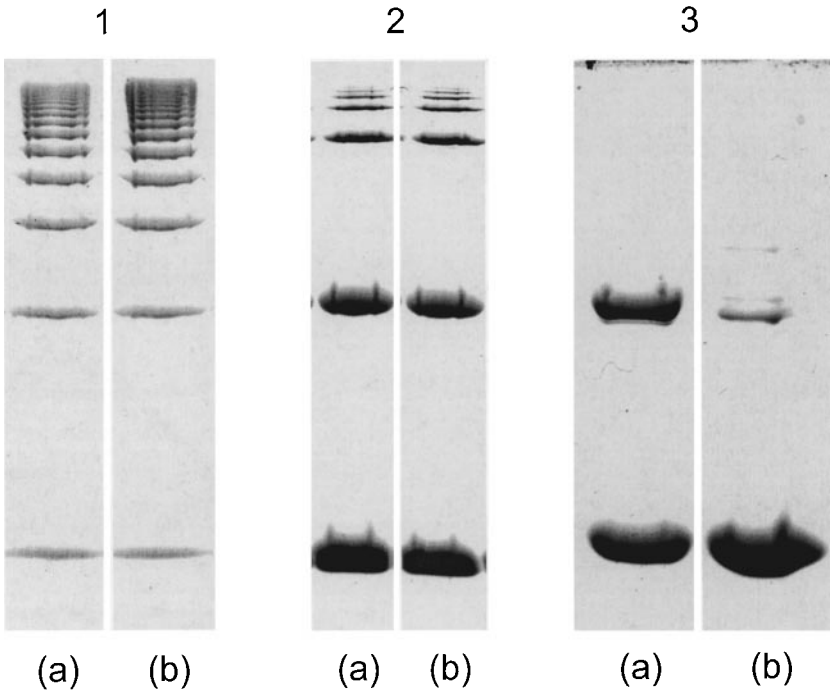

Figure 2. SDS-PAGE (non-reducing) of yeast F-actins cross-linked *via* disulfide formation and the reaction with dibromobimane. Panels 1-3 show the products of cross-linking Q41C (41-374), S265C (265-374), and Q41C/C374S-S265C/C374A (41-265) F-actins, respectively. The cross-linked cysteine residue pairs are indicated in parentheses. Q41C and S265C contain two reactive cysteine residues per monomer. Lanes (a) correspond to F-actins oxidized for two minutes in the presence of $CuSO_4$; lanes (b) show actins cross-linked by dibromobimane for 90 minutes (at 1:2 molar ratios of reagent to reactive cysteine residues on actin). Both reactions, in panels 1 and 2, reached maximum extent under these conditions.

F-actin. Three aspects of such a cross-linking should be noted. First, products larger than dimers cannot be formed because each actin monomer has only one reactive cysteine residue. Second, the cross-linking probability is reduced in the co-polymers in which not all of the neighbor pairs are suitable for this reaction. Third, the low level of co-polymer cross-linking by DBB may be explained by the inaccessibility of C265 and C41 in F-actin to DBB. The fact that a DBB-cross-linked dimer band is present in Figure 2 (panel 3) shows that such a reaction is feasible. In the other cross-linkings in Q41C and S265C F-actins, the initial DBB reactions with C374 proceed with little, if any, constraints.

Because the disulfide cross-linkings of cysteine residue pairs 41-374, 265-374, and 41-265 require much closer pair-wise proximity of these residues than is predicted in the models of F-actin structure, all cross-linked filaments were examined by electron microscopy. Moreover, the formation of disulfide bonds in the model F-actin structures was simulated in computations (see below). Figure 3 shows that the appearance and morphology of the disulfide cross-linked Q41C, S265C, and Q41C/C374S-S265C/C374A actin filaments is normal and does not reveal any major structural distortions, length limitations, or filament bundling. However, occasional sharp bends in the generally straight filaments were detected at higher frequency in Q41C F-actin (Figure 3(a)) than in other actins.

Modeling of cross-linked F-actin

The formation of disulfide bridges 41-265, 41-374, and 265-374 in the Lorenz (Lorentz *et al*., 1993) and Holmes (Holmes *et al*., 1990) models of F-actin was simulated as described in Materials and Methods. To assess the intra-monomer mobility of the three inter-monomer cross-linked sites in the filament, the structures of individual subunits of F-actin were extracted and superimposed with their corresponding initial conformations (i.e. the monomer structures in the Lorenz and Holmes F-actin models). The results of such a comparison and the measured relative rms deviations are shown in Figure 4.

The cross-linked sites exhibit considerable flexibility, but the movements remain localized in the exposed regions of the actin surface. The regions of induced conformational change are in the sequence vicinity of the cross-linked sites (Figure 4(d)), with a five-residue loop near position 167 as the sole exception to this pattern (in the case of the 41-265 cross-linked F-actin fitted to the Lorenz model, Figure 4(d)). A detailed inspection of the structures shown in Figure 4 reveals the following trends. First, the variability of residue 41 is consistently the smallest, and that of residue 374 is the largest, when structures of like origin are compared. The large movements (>10 Å) of the C terminus are consistent with the well-documented flexibility of this region (Orlova & Egelman, 1995). Second, the bridge with residue 374 induces a 2-3 Å larger movement in residue 265 than the bridge with residue 41. The 265-374 cross-linking, in particular, is not consistent with the β-hairpin conformation of the hydrophobic plug in the Lorenz structure (Figure 4(c)). Yet, it appears that this plug can detach from the main body of the protein and accommodate the 265-374 cross-linking in the Holmes model (Figure 4(a)). Third, it is evident from the comparison in Figure 4 that the Holmes model requires considerably less severe adjustments to the cysteine cross-bridges than the Lorenz model. The rms deviations of residue 41 in the Holmes model are negligible (<3 Å). Also, the movements of residue 265 and the C terminus are consistently (about 2 Å) smaller compared with those required by the Lorenz model.

Electron microscopy (EM) is the sole biophysical method that to date has yielded 3D images of intact actin filaments, albeit at low (20-35 Å) resolution (Milligan *et al*., 1990; Orlova & Egelman, 1993; Belmont *et al*. 1999; Bremer *et al*., 1994). The

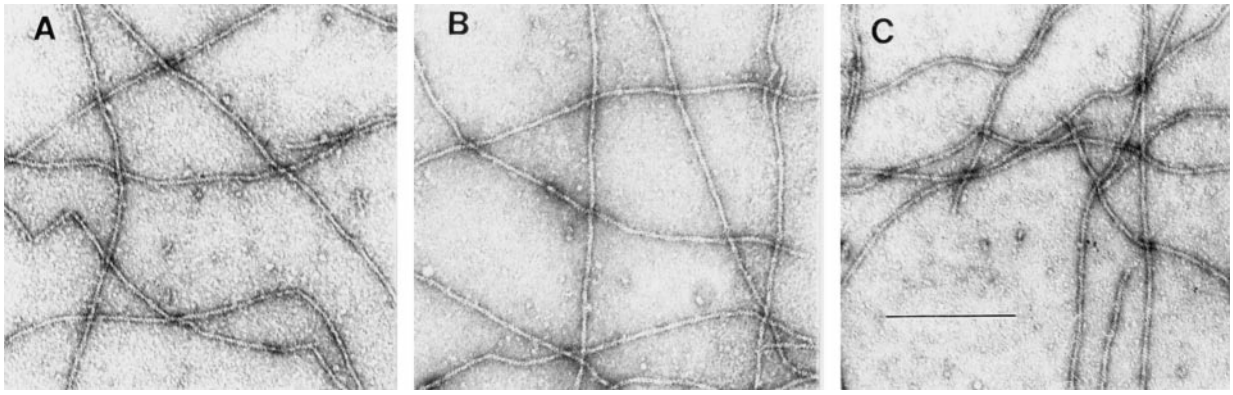

Figure 3. Electron micrographs of disulfide cross-linked yeast actin filaments. (a) Q41C (41-374), (b) S265C (265-374), and (c) Q41C/C374S-S265C/C374A (41-265) cross-linked F-actins. The bar represents 2000 Å. Samples were prepared for EM observation as described (Kim *et al*., 1998b).

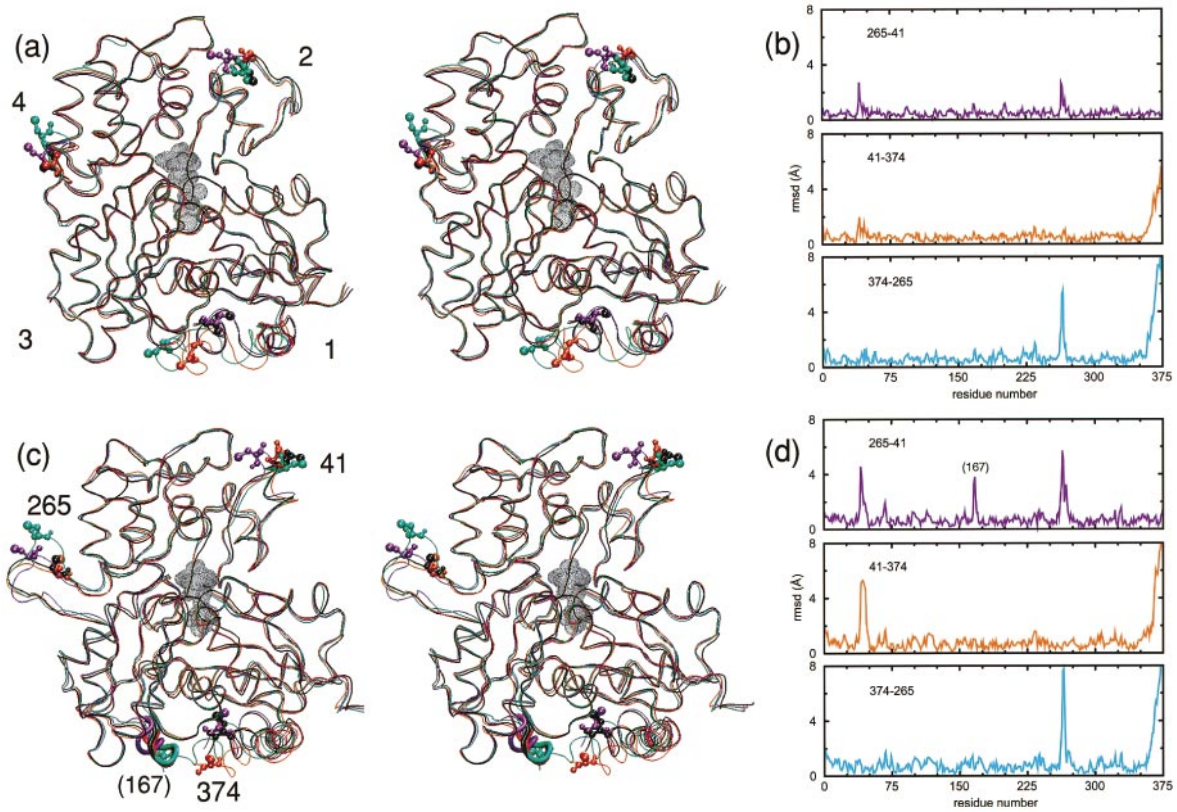

Figure 4. Conformational variability exhibited by simulated F-actin. (a) Stereo view of cross-linked subunits of the filament (individual monomers are superimposed) based on the Holmes model (Holmes *et al.*, 1990) and (b) corresponding rms deviations from the initial filament structure as a function of residue number. (c) Cross-linked subunits based on the Lorenz filament model (Lorenz *et al.*, 1993) and (d) corresponding backbone rms deviations in Ångstrom. The four structural subdomains (Kabsch *et al.*, 1990) of actin are denoted by numbers in (a). The three mutation sites, labeled in (c), are shown as ball-and-stick models. Also shown in (c) is loop 165-169 in tube representation. The color of the structures in (a), (c) codes for the cysteine residue cross-links enforced in the filament: 41-265 (violet), 41-374 (orange), 265-374 (turquoise). The original structure is shown in black. The protein is represented by backbone traces. Ca^{2+}-ADP is shown as black, transparent van-der-Waals spheres.

large magnitude of the predicted conformational change in actin's C terminus prompted the question of whether these changes could be observed by EM. To address this question, we lowered the resolution of the atomic models by applying a Gaussian filter (Wriggers *et al.*, 1998) to a level typically encountered in the microscope; the results for the 41-374 cross-linked F-actin are visualized in Figure 5. The low-resolution difference density map depicted in Figure 5(f) clearly identifies a shift of densities near the C terminus that would be observable by EM (Orlova & Egelman, 1995). The magnitude of the low-resolution density shifts was then measured by the maximum density variations in the difference density maps relative to the maximum density value of the original maps. For the predicted structures based on the Holmes model the following variations were measured: 4 % (41-265), 10 % (41-374), and 17 % (265-374). The corresponding values for the Lorenz-based models are: 5 % (41-265), 20 % (41-374), and 18 % (265-374). These values indicate that the 41-374 cross-linked F-actin (Figure 5) is particularly interesting, as this cross-linking should allow for a differentiation between the Lorenz and Holmes models. If the Lorenz model is correct, the cross-linking should induce a noticeable change in the low-resolution map of F-actin (Figure 5(f)). However, if the Holmes model is correct, the map should remain largely unaltered (Figure 5(c)). It may be noted that the 265-374 cross-linked F-actin (not shown) exhibited a density shift very similar to that shown in Figure 5(f).

Conclusions

Using yeast actin mutants with Gln41 and Ser265 substitutions to cysteine residues, we have documented intermonomer disulfide and dibromobimane cross-linking of F-actin between residue pairs 41-374, 265-374, and 41-265. These results support the hypothesis that the D-loop, C terminus, and H-plug cooperatively form an intermolecular interface in F-actin (Owen & DeRosier, 1993). The modeling of these cross-links into structures of F-actin can be achieved

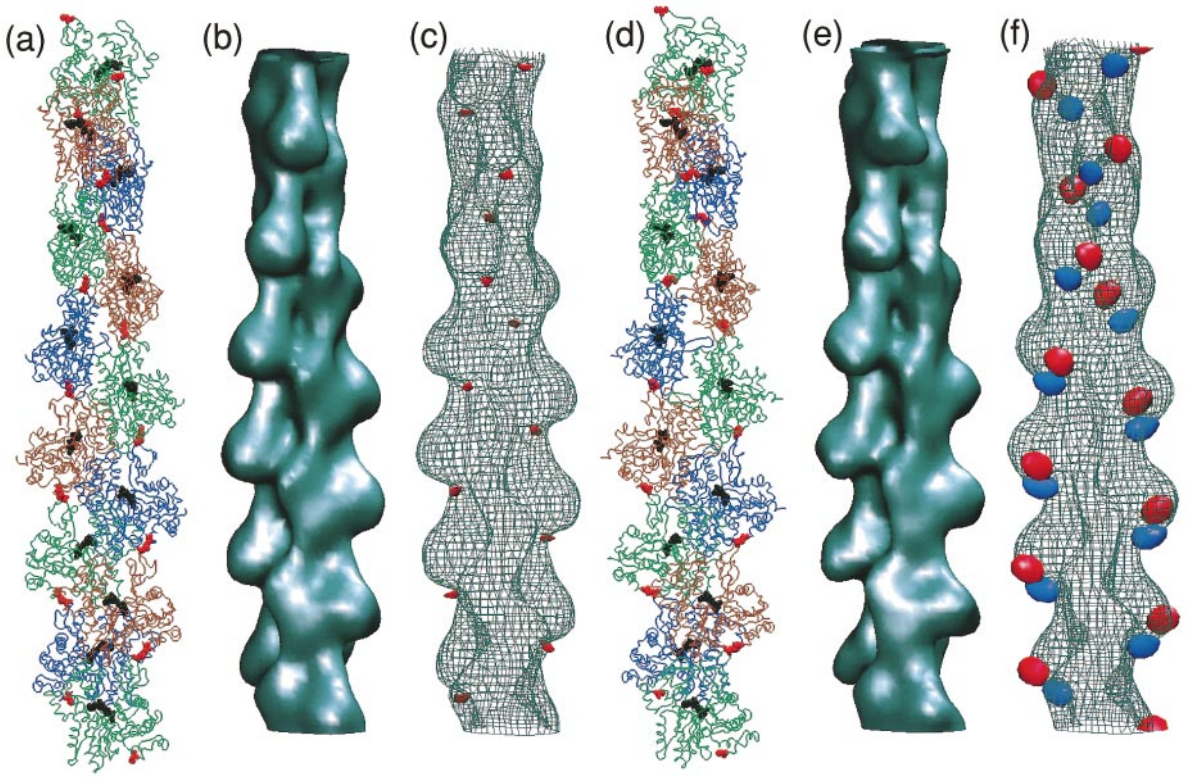

Figure 5. Multi-resolution rendering of conformational changes induced by the 41-374 disulfide bridge. (a) The Holmes model of F-actin after refinement. Individual monomers are shown as colored backbone traces, Ca^{2+}-ADP as black spheres. The 41-374 cross-bridges are shown in red. (b) Low-resolution map of the original Holmes model, shown as an isocontour at half-maximal density. The spatial resolution of the map (full-width half-maximum of the Gaussian kernel) is 13.6 Å (c) Low-resolution map of the refined model shown as a wire mesh, otherwise rendered as in (b). In addition, the difference density map relative to (b) is visualized by a red isocontour at −10 % of the maximum density value. Positive difference densities are below the +10 % density threshold. (d) The refined Lorenz model with the cross-linked sites (red). (e) Low-resolution map of the original Lorenz model, shown as an isocontour at half-maximal density. (f) Low-resolution map of the Lorenz model in the presence of the 41-374 cross-bridge shown as a wire mesh. The difference density map relative to (e) is visualized by isocontours at −10 % (red) and +10 % (blue) of the maximum density value. Figures 4 and 5 were created with the programs VMD (Humphrey *et al.*, 1996) and volcube (part of the Situs distribution; Wriggers *et al.*, 1999).

by allowing for flexible motions in the cross-linked regions, but it requires greater adjustments to the Lorenz than the Holmes model at these sites. If such adjustments are allowed, i.e. considerable rms deviations from model positions are permitted for residues located at the cross-linking sites, the overall Lorenz and Holmes models are compatible with the three cross-linkings reported here. However, we propose that EM image reconstruction analysis of 41-374 disulfide cross-linked F-actin should differentiate between the Holmes and Lorenz models of F-actin.

Materials and Methods

Materials

The QuikChange™ site-directed mutagenesis kit, DNA restriction enzymes, and plasmid purification kit were purchased from Stratagene (La Jolla, CA), New England Biolabs (Beverly, MA) and Qiagen (Valencia, CA), respectively. Peptone, tryptone and yeast extract were from Difco (Detroit, MI). DNase I was purchased from Worthington Biochemical Corporation (Lakewood, NJ).

Oligonucleotide-directed mutagenesis

The mutagenesis was performed according to Stratagene (La Jolla, CA) QuikChange procedure using oligonucleotides purchased from Genset Corp. (San Diego, CA). As a template for mutagenesis we used double stranded yeast shuttle plasmid pTD24 (Miller *et al.*, 1996), which carries a copy of the ACT1 gene. Two oligonucleotide primers, 5′-CCAAGACACtgtGGTATCATG GTCGG-3′ and 5′-CCGACCATGATACCacaGTGTC TTGG-3′, were used to introduce the Q41C actin mutation. Two primers, 5′-CAGAGATTAGAAgcttT TGTGGTGAAC-3′ and 5′-GTTCACCACAAaagcTTC-TAATCTCTG-3′ were used to generate the C374S actin mutation. The mutated sequences are shown in lowercase and selective restriction enzyme markers are underlined (In Q41C the *Sty*I site is lost while in C374S the *Hin*dIII site is added). Actin genes from screened plasmid clones were sequenced (GeneMed, San Francisco, CA) to confirm the absence of random errors.

Yeast transformation

Mutant plasmids carrying HIS3 marker were transformed into the diploid yeast strain TDS101 (Miller *et al*., 1996) that has a single ACT1 gene copy on the plasmid with URA3 marker and genomic copies of ACT1 gene deleted. The original plasmid carrying ACT1 gene was sorted out by plasmid shuffling (Sikorsky *et al*.,1995). The cells were screened for HIS plus and URA minus phenotype, which resulted in yeast cells carrying a homozygous copy of mutant actin gene.

Purification of yeast actin

Yeast actin was purified by affinity chromatography on DNase I column as described (Cook *et al*., 1993). To avoid a possible contamination of yeast actin with cofilin, the DNase I column was washed with 1.0 M NaCl (Du & Frieden, 1982) in G-actin buffer (10 mM Tris-HCl (pH 7.8), 1.0 mM DTT, 0.2 mM ATP and 0.2 mM $CaCl_2$) prior to the elution of yeast actin. With this additional purification step, we did not observe any protein contamination in the yeast actin preparations.

Cross-linking of actin and SDS-PAGE analysis

Purified G-actin was stored in 10 mM Tris-HCl (pH ~ 8.0), 0.2 mM $CaCl_2$, 0.2 mM ATP, 1.0 mM DTT, under nitrogen and on ice. Prior to cross-linking reactions, DTT was removed from G-actin by passing it through Sephadex G-50 spin columns equilibrated with 5.0 mM bis-Tris (pH 6.0), 0.2 mM $CaCl_2$, and 0.2 mM ATP. The G-actin was then polymerized for 15 minutes with 2.0 mM $MgCl_2$. The low pH (6.0) level prevents disulfide cross-linking of actin during the polymerization reaction. The disulfide cross-linking was catalyzed by raising the pH to approximately 7.5 (by adding 1.0 M Tris buffer at pH 8.0 to 15 mM) and by the addition of 50 μM $CuSO_4$. Such reactions reach plateau levels of cross-linking within one minute. In the absence of $CuSO_4$, the same reactions take between 12 and 15 hours to reach similar levels of cross-linking. The spontaneous disulfide formation is greatly accelerated if DTT is removed from G-actin by overnight dialysis rather than over spin columns. The partially oxidized actin produced during such a dialysis reaches maximum levels of cross-linking within 60 to 80 minutes. The dibromobimane cross-linking was initiated by adding this reagent to F-actin (at 1:2 molar ratio of DBB to reactive cysteine residues on actin) obtained *via* the spin column procedure. Spontaneous disulfide cross-linking in such an actin was slow and did not exceed few percentages of the total cross-linking in the DBB reaction (see above). All cross-linking reactions were stopped by adding 3.0 mM *N*-ethylmaleimide and SDS electrophoresis sample buffer (without β-mercaptoethanol) to block the unreacted cysteine residues on actin. The actin samples were then boiled and analyzed by SDS-PAGE. Protein bands were visualized by Coomassie staining and by UV fluorescence in the case of DBB cross-linked actin.

Modeling of cross-linked F-actin

F-actin models were constructed using helical symmetry parameters (Holmes *et al*., 1990; Lorenz *et al*., 1993). The initial structures of actin (Lorenz *et al*., 1993; McLaughlin *et al*., 1993) were kindly provided by Paul McLaughlin and Michael Lorenz. The missing D-loop was added to the monomer structure as described (Wriggers & Schulten, 1999). The molecular mechanics calculations described in this paper were carried out with X-PLOR (Brünger, 1992) using default parameters of the CHARMM united atom force field (Brooks *et al*., 1983) version 19, for the protein and non-bonded interactions. A total of 32 water molecules per monomer (Wriggers & Schulten, 1999) plus two additional molecules per monomer filling the empty ATP γ-phosphate cavity, were placed into the Holmes model of F-actin to maintain the stability of actin's nucleotide binding pocket. The Lorenz model of F-actin was used unaltered without explicit water. Explicit water molecules were simulated using the TIP3(P) water model (Jorgensen *et al*., 1983); all other solvent effects were simulated using the standard distance-dependent dielectric constant provided by X-PLOR (Brünger, 1992). ADP and Ca^{2+} was simulated using default parameters of the CHARMM all-atom force field, version 22 (MacKerell Jr. *et al*., 1992; Pavelites *et al*., 1997). The Q41C and S265C mutations were modeled with X-PLOR.

Powell energy minimization (Brünger, 1992) was carried out to enforce the disulfide bridges 41-265, 41-374, and 265-374, in the Lorenz and Holmes models of the filament. This optimization method was favored over more extensive molecular dynamics protocols to avoid introducing thermal disorder in the structures. Our main goal was to conserve the original structures as much as possible while relaxing the conformation near the newly built cross-links. This allowed us to estimate the degree to which the original structures were consistent with the conformational constraints introduced by the disulfide bridges. Cross-links were formed between seven adjacent monomers on the F-actin helix. The total size of the simulated F-actin heptamers was 25,949 atoms for the Holmes-based models, and 25,235 atoms for the Lorenz-based models. In a first round of energy minimization, each heptamer was optimized using 2000 Powell steps. Cross-links at C374 induced a shift of the C-terminal residues that disrupted the hydrogen bonds of the C-terminal α-helix (see below). To alleviate the strain in the C terminus, heptamers including cross-links at C374 were minimized in a second round (2000 Powell steps) of energy minimization. At the beginning of this second round, the displacement of the C terminus was ''smoothed'' between positions 357-374 by applying the displacement vector measured at residue 374 with a magnitude linearly proportional to the distance in sequence from residue 357 at the start of the C-terminal helix. The helical symmetry of the F-actin heptamer was maintained by helical projection of the motions exhibited by the central monomer every 1000 steps of minimization.

The atomic coordinates of the cross-linked F-actin models are available by FTP. E-mail: wriggers@scripps.edu.

Acknowledgments

This work was supported by awards from the NIH and NSF to E.R. and from the NIH to P.A.R. W.W. was supported in part by awards from NIH to Charles L. Brooks, III, Ronald A. Milligan and J. Andrew McCammon, and by the LJIS fellowship program/Burroughs Wellcome Fund.

References

Belmont, L. D., Orlova, A., Drubin, D. G. & Egelman, E. H. (1999). A change in actin conformation associated with filament instability after P-i release. *Proc. Natl Acad. Sci. USA,* **96**, 29-34.

Bremer, A., Henn, C., Goldie, K. N., Engel, A., Smith, P. R. & Aebi, U. (1994). Towards atomic interpretation of F-actin filament three-dimensional reconstructions. *J. Mol. Biol.* **242**, 683-700.

Brooks, B., Bruccoleri, R., Olafson, B., States, D., Swaminathan, S. & Karplus, M. (1983). CHARMM: a program for macromolecular energy, minimization, and dynamics calculations. *J. Comp. Chem.* **4**, 187-217.

Brünger, A. (1992). *X-PLOR, Version 3.1: A System for X-ray Crystallography and NMR.* The Howard Hughes Medical Institute and Department of Molecular Biophysics and Biochemistry, Yale University, USA.

Chik, J. K., Lindberg, U. & Schutt, C. E. (1996). The structure of an open state of beta-actin at 2.65 Å resolution. *J Mol. Biol.* **263**, 607-623.

Cook, R. K., Root, D., Miller, C., Reisler, E. & Rubenstein, P. A. (1993). Enhanced stimulation of myosin subfragment-1 ATPase activity by addition of negatively charged residues to the yeast actin NH_2-terminus. *J. Biol. Chem.* **268**, 2410-2415.

Du, J. & Frieden, C. (1998). Kinetic studies on the effect of yeast cofilin on yeast actin polymerization. *Biochemistry,* **37**, 13276-13284.

Feng, L., Kim, E., Lee, W. L., Miller, C. J., Kuang, B., Reisler, E. & Rubenstein, P. A. (1997). Fluorescence probing of yeast actin subdomain 3/4 hydrophobic loop 262-274: actin-actin and actin-myosin interactions in actin filaments. *J. Biol. Chem.* **272**, 16829-16837.

Hegyi, G., Premecz, G., Sain, B. & Muhlrad, A. (1974). Selective carboethoxylation of the histidine residues of actin by diethylpyrocarbonate. *Eur. J. Biochem.* **44**, 7-12.

Hegyi, G., Mak, M., Kim, E., Elzinga, M., Muhlrad, A. & Reisler, E. (1998). Intrastrand cross-linked actin between Gln41 an Cys374. I. Mapping of sites cross-linked in F-actin by *N*-(4-azido-2-nitrophenyl) putrescine. *Biochemistry,* **37**, 17784-17792.

Holmes, K. C., Popp, D., Gebhard, W. & Kabsch, W. (1990). Atomic model of the actin filament. *Nature,* **347**, 44-49.

Humphrey, W., Dalke, A. & Schulten, K. (1996). VMD - visual molecular dynamics. *J. Mol. Graph.* **14**, 33-38.

Jorgensen, W. L., Chandrasekhar, J., Madura, J. D., Impey, R. W. & Klein, M. L. (1983). Comparison of simple potential functions for simulating liquid water. *J. Chem. Phys.* **79**, 926-935.

Kabsch, W., Mannherz, H. G., Suck, D., Pai, E. F. & Holmes, K. C. (1990). Atomic structure of the actin-DNase-I complex. *Nature,* **347**, 37-44.

Khaitlina, S. Y., Moraczewska, J. & Strzelecka-Golaszewska, H. (1993). The actin/actin interactions involving the N terminus of the DNase-I-binding loop are crucial for stabilization of the actin filament. *Eur. J. Biochem.* **218**, 911-920.

Kim, E., Bobkova, E., Miller, C. J., Orlova, A., Hegyi, G., Egelman, E. H., Muhlrad, A. & Reisler, E. (1998a). Intrastrand cross-linked actin between Gln41 and Cys374. III. Inhibition of motion and force generation with myosin. *Biochemistry,* **37**, 17801-17809.

Kim, E., Miller, C. J., Motoki, M., Seguro, K., Muhlrad, A. & Reisler, E. (1996). Myosin-induced changes in F-actin - fluorescence probing of subdomain 2 by dansyl ethylenediamine attached to Gln41. *Biophys. J.* **70**, 1439-1446.

Kim, E., Phillips, M., Hegyi, G., Muhlrad, A. & Reisler, E. (1998b). Intrastrand cross-linked actin between Gln41 and Cys374. II. Properties of cross-linked oligomers. *Biochemistry,* **37**, 17793-17800.

Kim, E. & Reisler, E. (1996). Intermolecular coupling between loop 38-52 and the C terminus in actin filaments. *Biophys. J.* **71**, 1914-1919.

Lorenz, M., Popp, D. & Holmes, K. C. (1993). Refinement of the F-actin model against X-ray fiber diffraction data by the use of a directed mutation algorithm. *J. Mol. Biol.* **234**, 826-836.

MacKerell, A. D., Jr, Bashford, D., Bellott, M., Dunbrack, R. L., Jr., Evanseck, J., Field, M. J., Fischer, S., Gao, J., Guo, H., Ha, S., Joseph, D., Kuchnir, L., Kuczera, K., Lau, F. T. K., Mattos, C., *et al.* (1992). Self-consistent parameterization of biomolecules for molecular modeling and condensed phase simulations. *FASEB J.* **6**, A143.

McLaughlin, P. J., Gooch, J. T., Mannherz, H. G. & Weeds, A. G. (1993). Structure of gelsolin segment-1-actin complex and the mechanism of filament severing. *Nature,* **364**, 685-692.

Miller, C. J., Doyle, T. C., Bobkova, E., Botstein, D. & Reisler, E. (1996). Mutational analysis of the role of hydrophobic residues in the 338-348 helix on actin in actomyosin interactions. *Biochemistry,* **35**, 3670-3676.

Milligan, R. A., Whittaker, M. & Safer, D. (1990). Molecular structure of F-actin and location of surface binding sites. *Nature,* **348**, 217-221.

Muhlrad, A., Cheung, P., Phan, B. C., Miller, C. & Reisler, E. (1994). Dynamic properties of actin - structural changes induced by beryllium fluoride. *J. Biol. Chem.* **269**, 11852-11858.

Orlova, A. & Egelman, E. H. (1993). A conformational change in the actin subunit can change the flexibility of the actin filament. *J. Mol. Biol.* **232**, 334-341.

Orlova, A. & Egelman, E. H. (1995). Structural dynamics of F-actin. I. Changes in the C terminus. *J. Mol. Biol.* **245**, 582-597.

Owen, C. & DeRosier, D. (1993). A 13 Å map of the actin-scruin filament from the limulus acrosomal process. *J. Cell Biol.* **123**, 337-344.

Pavelites, J. J., Gao, J. L., Bash, P. A. & Mackerell, A. D. (1997). A molecular mechanics force field for NAD(+), NADH, and the pyrophosphate groups of nucleotides. *J. Comp. Chem.* **18**, 221-239.

Rayment, I., Holden, H. M., Whittaker, M., Yohn, C. B., Lorenz, M., Holmes, K. C. & Milligan, R. A. (1993). Structure of the actin-myosin complex and its implications for muscle contraction. *Science,* **261**, 58-65.

Squire, J. M. & Morris, E. P. (1998). A new look at thin filament regulation in vertebrate skeletal muscle. *FASEB J.* **12**, 761-771.

Schwyter, D. H., Kron, S. J., Toyoshima, Y. Y., Spudich, J. A. & Reisler, E. (1990). Subtilisin cleavage of actin inhibits *in vitro* sliding movement of actin filaments over myosin. *J. Cell Biol.* **111**, 465-470.

Schröder, R. R., Manstein, D. J., Jahn, W., Holden, H., Rayment, I., Holmes, K. C. & Spudich, J. A. (1993). Three-dimensional atomic model of F-actin decorated with *Dictyostelium* myosin S1. *Nature,* **364**, 171-174.

Sikorski, R. S. M., William, A., Tugendreich, S. & Hieter, P. (1995). Allele shuffling: conjugational transfer, plasmid shuffling and suppressor analysis in *Saccharomyces cerevisiae*. *Gene*, **155**, 51-59.

Tirion, M. M., ben-Avraham, D., Lorenz, M. & Holmes, K. C. (1995). Normal modes as refinement parameters for the F-actin model. *Biophys. J.* **68**, 5-12.

Wriggers, W. & Schulten, K. (1999). Investigating a back door mechanism of actin phosphate release by steered molecular dynamics. *Proteins: Struct. Funct. Genet.* **35**, 262-273.

Wriggers, W., Milligan, R. A., Schulten, K. & McCammon, J. A. (1998). Self-organizing neural networks bridge the biomolecular resolution gap. *J. Mol. Biol.* **284**, 1247-1254.

Wriggers, W., Milligan, R. A. & McCammon, J. A. (1999). Situs: a package for docking crystal structures into low-resolution maps from electron microscopy. *J. Struct. Biol.* **125**, 185-195.

Edited by M. F. Moody

(Received 24 December 1999; received in revised form 23 March 2000; accepted 27 March 2000)